7
Real-Time, Ultra-Low-Level Detection of Hg^{2+} Ions by MoS_2 Functionalized AlGaN/GaN HEMT for Water Analysis

This chapter provides a description related to the development of an AlGaN/GaN HEMT sensor to detect the highly toxic mercury (Hg^{2+}) ions in the aqueous medium. Here, the gate region of the AlGaN/GaN HEMT is functionalized with hydrothermally grown MoS_2. In this chapter, the development and sensing of Hg^{2+} ions using MoS_2 functionalized AlGaN/GaN HEMT is explained by unwrapping each step. These steps contain the description of hydrothermal growth of MoS_2, its morphological characterization, its functionalization over the gate terminal of AlGaN/GaN HEMT, and the corresponding electrical characterization for the sensing of Hg^{2+} ions.

7.1 INTRODUCTION

Mercury (Hg) has been recognized as one of the most known toxic metals as its trace amount also potentially dangerous. It causes both chronic and acute poisoning, and excessive exposure causes severe health problems such as irreversible neurological damage, cancer, and motion disorders that can lead to death [Chen *et al.*, 2012b; Sayyah *et al.*, 2016]. To prevent the toxicity of Hg^{2+} ions in water, the concentration of Hg^{2+} ions should be below the guideline values of WHO (1 ppb) and EPA (2 ppb) [Cho *et al.*, 2010; Gumpu *et al.*, 2015]. Thus, it is necessary to rapidly and efficiently monitor mercury at trace levels in the drinking water and other water bodies.

Significant efforts have been made for the detection of the mercury at trace levels by various analytical approaches. These methods include optical analysis like colorimetric and spectroscopic techniques [Bettini *et al.*, 2014; Cho *et al.*, 2010], electrochemical techniques such as amperometry, and voltammetry [Arduini *et al.*, 2011; Gong *et al.*, 2010]. These approaches show good sensitivity but are expensive, time-consuming, complicated, and laboratory-based approaches, which require specific operators for analysis [Jia *et al.*, 2016]. Methods like ion-selective electrodes (ISE) using gold (Au) as an electrode have advantages that they can provide higher sensitivity and reasonable detection limits for different ion sensing applications. However, these Au electrodes need a specific configuration, a filling solution, and a reference electrode. This configuration limits its extensive use in ion sensing. The Si-based ion-sensitive field-effect transistors (ISFETs) were utilized to solve the portability and robustness problems related to Au electrodes [Chen *et al.*, 2012a]. However, the chemical instability in ionic solutions and the necessity of the reference electrode not only limits the performance of the Si-ISFETs but restricts the miniaturization of the device as well [Asadnia *et al.*, 2016].

AlGaN/GaN HEMTs with its superior material characteristics like higher chemical and thermal stability, wide bandgap, and piezoelectric and spontaneous polarization properties provide an efficient way to develop the AlGaN/GaN HEMT based ion sensors. AlGaN/GaN HEMTs possess two-dimensional electron gas (2DEG) at the heterointerface of AlGaN and GaN due to their spontaneous and piezoelectric polarization properties [Chen *et al.*, 2008]. The presence of 2DEG at the channel region makes the device normally-on, which makes it a reference electrode free device and favors further miniaturization of the device. In comparison to Si-ISFETs,

AlGaN/GaN HEMTs have several advantages. In enhancement mode Si-ISFETs, a reference electrode is required to provide gate potential above the threshold voltage to form a channel, whereas the AlGaN/GaN HEMTs can efficiently work as reference electrode free devices. The depletion-mode Si-ISFETs possess very less mobility and carrier concentration compared to AlGaN/GaN HEMTs; therefore, the AlGaN/GaN HEMT based ion sensors can provide 100 times better performance than Si-ISFETs [Zhang *et al.*, 2019]. Moreover, the electron density at 2DEG is highly sensitive for any change at the gate region compared to Si-ISFETs. Hence, the AlGaN/GaN HEMTs have superior advantages over other ion sensors to attain excellent sensitivity and miniaturization without reference electrode utilization.

The AlGaN/GaN HEMTs were used as chemical and biosensors for the detection of various elements such as glucose, prostate-specific antigens, and ions like mercury, cadmium, and nitrate [Asadnia *et al.*, 2016; Myers *et al.*, 2013; Nigam *et al.*, 2019b; Wang *et al.*, 2007]. These sensors showed rapid response time with excellent sensitivity at trace levels. Therefore, some studies for Hg^{2+} ion detection were also carried out using AlGaN/GaN HEMT based sensors. Wang et al. compared bare Au and the Au with thioglycolic acid functionalization on AlGaN/GaN HEMTs to detect Hg^{2+} ions and achieved fast response time below 5 s and 27 ppb detection limit for Hg^{2+} ions [Wang *et al.*, 2007]. Asadnia *et al.* reported polyvinyl chloride (PVC) functionalized AlGaN/GaN HEMT sensor to detect Hg^{2+} ions observed the limit of detection of 10^{-8} M [Asadnia *et al.*, 2016]. Besides this, Chen et al. utilized the AlGaN/GaN HEMT for detection of low concentration of Hg^{2+} ions using the thioglycolic acid-functionalized gate and have observed a good limit of detection of 1.5×10^{-8} M, a magnitude lower than their previous work (10^{-7} M to 10^{-8} M) [Chen *et al.*, 2008; Wang *et al.*, 2007]. This lower detection of Hg^{2+} ions is required for many applications. These reports suggest the vast applicability of AlGaN/GaN HEMTs for Hg^{2+} ion detection.

In the last few years, MoS_2, a transition metal dichalcogenide, has got much attraction owing to its distinct electrical, optical, chemical, and mechanical properties such as tunable bandgap and high surface to volume ratio [Kumar *et al.*, 2018]. So far, several research groups have synthesized MoS_2 by different processes like mechanical exfoliation [Goel *et al.*, 2018], chemical vapor deposition [Kumar *et al.*, 2018], sulfurization of Mo or MoO_3 [Kumar *et al.*, 2018; Taheri *et al.*, 2016], and hydrothermal process [Feng *et al.*, 2015; Zheng *et al.*, 2018] and prepared several morphologies of MoS_2 in the form of different micro and nanostructures [Feng *et al.*, 2015; Kumar *et al.*, 2018; Wu *et al.*, 2016b] for the widespread sensing applications [Aswathi and Sandhya, 2018; Goel *et al.*, 2018]. Among different micro and nanostructures of MoS_2, the three-dimensional (3D) micro and nanostructures such as flowers and flower-like structures have received much attention because of their unique structural properties.

There were several nanosheets gathered together to form the flower-like structures, which can increase the number of adsorption sites on the sensing surface and results in the enhanced sensitivity of the sensors for different sensing applications [Feng *et al.*, 2015]. Moreover, the remarkable advantages of flower-like structures have plenty of active edges that play a prominent role in electrochemical reactions [Yifei Guo *et al.*, 2017]. In addition, the higher catalytic activity was also observed in flower-like structures compared to basal plane MoS_2 films, which can improve the sensitivity of the sensors [Cho *et al.*, 2015]. Some research groups also observed the applicability of MoS_2 in Hg^{2+} ions detection. Jia et al. demonstrated MoS_2 as an excellent adsorbent of Hg^{2+} ions to remove them from water and showed adsorption studies of Hg^{2+} ions on natural MoS_2 using atomic force microscopy (AFM) [Jia *et al.*, 2017a; Jia *et al.*, 2017b]. Aswathi et al. reported solvent exfoliated synthesis of MoS_2 for Hg^{2+} ion sensing by an electrochemical route and observed ultra-low-level detection of Hg^{2+} ions [Aswathi and Sandhya, 2018]. Liu et al. explain the detection of Hg^{2+} ions by MoS_2 nanosheet as fluorescent probes with boron and nitride doping [Liu *et al.*, 2015]. These reports showed the suitability of MoS_2 for low-level Hg^{2+} ion detection.

7.2 MATERIALS UTILIZED IN THE EXPERIMENTS

The materials utilized here are Molybdenum (VI) oxide (MoO_3), Thiourea (CH_4N_2S), NaOH for the hydrothermal process of MoS_2. The NaH_2PO_4, Na_2HPO_4 were used here for the preparation of phosphate buffer solution. Other reagents such as $Hg(NO_3)_2.H_2O$, $Cr(NO_3)_3.9H_2O$ $CuSO_4$, $Cd(NO_3)_2.4H_2O$, $Ni(NO_3)_2.6H_2O$, $Zn(NO_3)_2.6H_2O$, $Pb(NO_3)_2$ were employed for the development of ionic solutions of respective metals for sensing analysis.

7.3 HYDROTHERMAL SYNTHESIS OF MoS_2

The synthesis of MoS_2 was carried out by the simple hydrothermal process and is showed in Figure 7.1. In this process, MoO_3, NaOH, and CH_4N_2S were used as precursor materials in the ratio 0.6:0.2:2 g, respectively. The homogenous solution of these materials was prepared by mixing them in the prescribed ratio in 40 ml DI (deionized) water through continuous stirring for 1 h. The stirred mixture was moved in 50 ml Teflon lined hydrothermal autoclave and heated at 200°C for 24 hours. By this method, a black colored solution was obtained and rinsed many times by DI water. Further, this black colored product was centrifuged. Due to centrifugation, the black precipitates were settled on the ground. These precipitates were filtered and then dried at 80°C till 1 h in the oven. This process results in black colored MoS_2 powder [Nigam *et al.*, 2020].

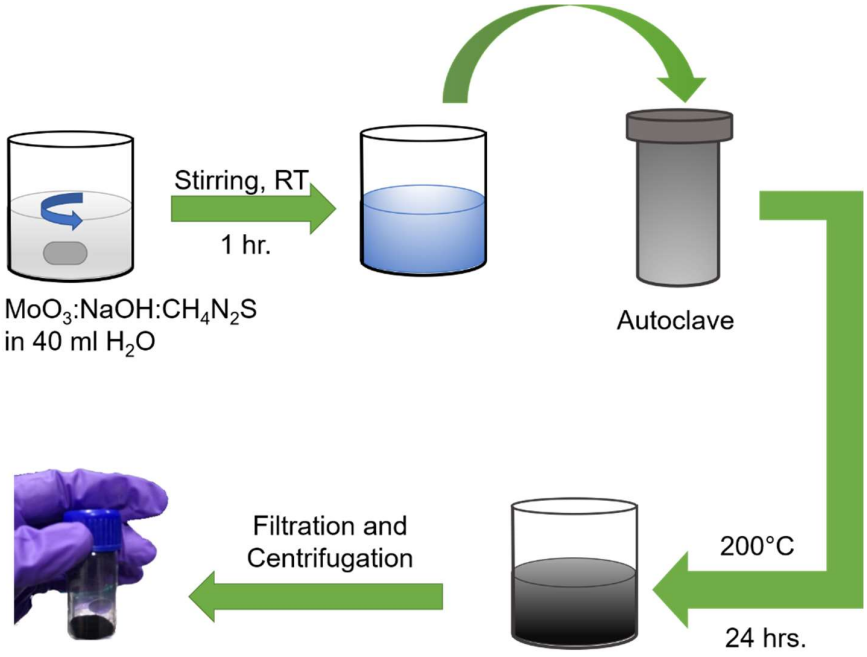

Figure 7.1: Hydrothermal synthesis process of MoS_2 using MoO_3, CH_4N_2S, and NaOH

7.4 PREPARATION OF MOS_2 FUNCTIONALIZED AlGaN/GaN HEMT ION SENSOR

The HEMT fabrication process was described in detail in chapter 4. After the fabrication of AlGaN/GaN HEMT and synthesis of MoS_2, the gate region of HEMT was functionalized by self-assembled MoS_2 layers. In this approach, the as-synthesized MoS_2 powder was ground for 30 minutes. After grinding, a solution of 20 mg/ml was prepared in IPA (isopropyl alcohol) of MoS_2 powder. This solution was ultrasonicated for 2 hrs. Subsequently, this solution was drop cast on the gate region of the HEMT. After that, the device was annealed for 15 minutes at 80°C. In this process, when MoS_2 forms a layer on the gate terminal, it adsorbed on the Au-gated HEMT [Nigam *et al.*, 2020].

7.5 MEASUREMENT AND CHARACTERIZATION

The crystalline nature and phases of the MoS_2 were examined using an X-ray diffraction approach (*X*RD) on an *X*-ray diffractometer. The MoS_2 morphologies were identified using field-emission scanning electron microscopy (FESEM) of Tecnai G^2 20 (FEI) S-Twin. Further, the vibrational spectrum of the MoS_2 was observed by performing the Raman spectroscopy. After the functionalization of MoS_2 on the gate region of AlGaN/GaN HEMT, the electrical characterizations were performed using the Keithley-4200 semiconductor characterization system [Nigam *et al.*, 2020]. The detection of the Hg^{2+} ions was observed by performing a similar process, as explained in chapters 5 and 6. In this work, the range of Hg^{2+} ion concentration was used from 0.1 ppt to 10 ppm for experimental analysis. The phosphate buffer saline solution (PBS buffer) was utilized for the preparation of Hg^{2+} and other heavy metal ion solutions. The pH of the solutions was kept constant at 7.

7.6 PREPARATION OF SOLUTIONS OF DIFFERENT CONCENTRATIONS OF Hg^{2+} IONS

In order to detect Hg^{2+} ions at different concentrations, a stock solution of Hg^{2+} ions of 100 ppm was prepared by adding 2.56 mg $Hg(NO_3)_2.H_2O$ in a 15 ml phosphate buffer solution[Nigam *et al.*, 2020]. The stock solution was diluted for different solution range by using the solution dilution equation:

$$M_1V_1=M_2V_2 \tag{7.1}$$

where M_1, V_1 represents the concentration and volume of stock solution, respectively, and M_2 and V_2 are the desired concentration and volume of the required solution, respectively. This equation estimates the volume of stock or higher concentration solution that should be added in the solvent to realize a specified concentration solution of Hg^{2+} ions. By utilizing the Eq. (7.1), solutions of different Hg^{2+} ions from 10 ppm to 0.1 ppt were prepared [Nigam *et al.*, 2020]. The concentration of as-prepared solutions was verified by performing atomic absorption spectroscopy (AAS) on three different concentrations of Hg^{2+} ions (0.1 ppb, 1 ppb, and 10 ppb), and the results were shown in Table 7.1. The analysis reveals the excellent agreement between as-prepared solutions and AAS measurement, and hence the solution preparation procedure of the different concentrations of Hg^{2+} ions has been verified.

Table 7.1: Concentration analysis of Hg^{2+} ions

Concentration of Hg^{2+} ions in as prepared solutions (ppb)	*Concentration observed by AAS (ppb)*
0.1	0.103
1	1.061
10	10.049

7.7 STRUCTURAL ANALYSIS OF MoS_2

7.7.1 SEM Analysis

The scanning electron microscopy (SEM) was performed to analyze the morphology of as-synthesized MoS_2. Figure 7.2 (a) shows a generalized view of SEM results of MoS_2 structures, and the magnified view showed in Figure 7.2 (b). These results reveal the formation of uniform flower-like MoS_2 nanostructures. Figure 7.2 (b) demonstrates that the nanostructures consist of many curved nanoflakes or nano-petals with a length of several nanometers. These nano-petals are very thin and can form relatively open and porous nanostructures, which makes excellent use of the grain surfaces that are easily accessible to the ionic solutions [Nigam *et al.*, 2020]. These porous nanostructures can also beneficial for electron transport during ion sensing [Wang *et al.*, 2018].

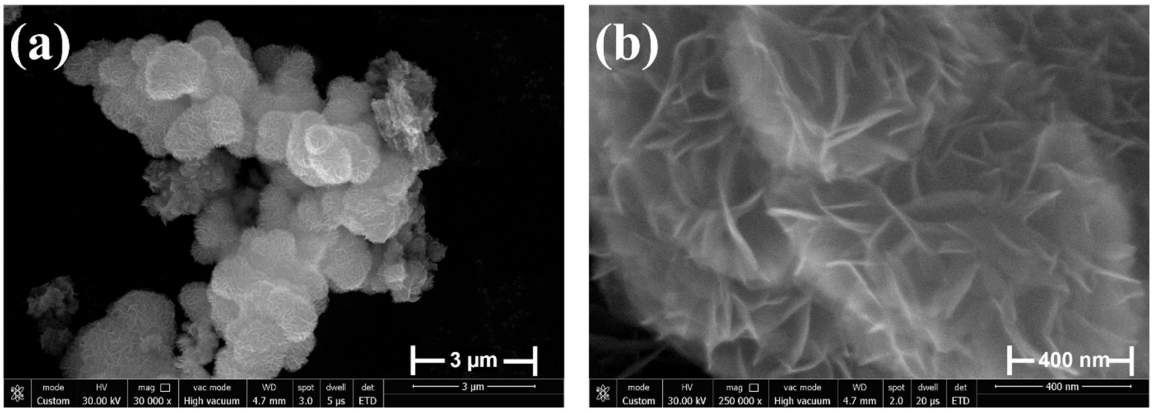

Figure 7.2: SEM images of (a) MoS_2 flower-like structures, (b) magnified view of MoS_2 flower-like structures.

7.7.2 XRD and Raman Analysis of MoS_2

The X-ray diffraction (XRD) pattern of the as-prepared MoS_2 flower-like structures prepared by the hydrothermal route is depicted in Figure 7.3. The XRD peaks observed at 2θ = 14.124, 33.465, 39.36 and 58.688 represents the (002), (100), (103) and (110) phase of MoS_2 respectively (JCPDS - 37-1492) [Liu *et al.*, 2015; Wang *et al.*, 2018]. It can be realized that the diffraction peak at 2θ = 14.124 is higher than other phases, which indicate that the flower-like MoS_2 structures show good crystalline behavior towards the (002) phase of MoS_2 and the structure is well developed [Nigam *et al.*, 2020]. In the XRD pattern, there were no impurity peaks observed, which means a pure MoS_2 was formed by the hydrothermal route.

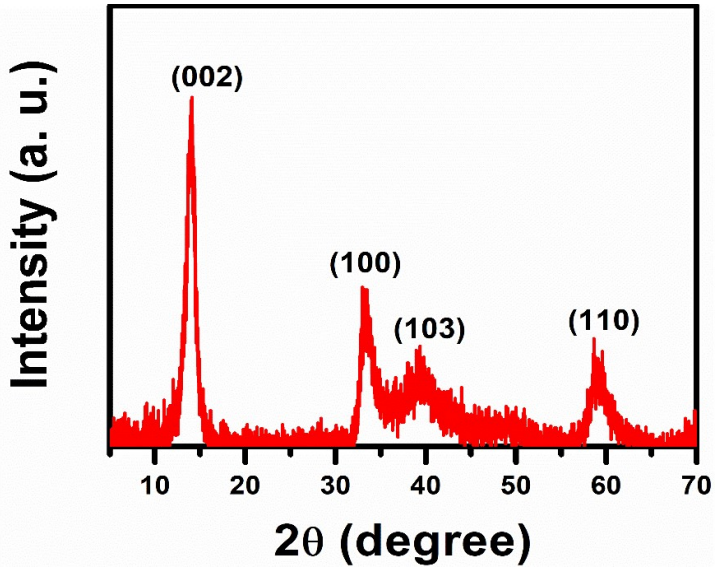

Figure 7.3: XRD pattern of the flower-like MoS_2

Further, the Raman analysis of the as-prepared MoS_2 was also performed at room temperature, and it is shown in Figure 7.4. Raman spectra explain about the thickness and layer alignment of the synthesized MoS_2. There were two peaks observed at 376 and 401 cm^{-1}, which attributes the E_{2g}^1, and A_{1g} vibration modes of MoS_2, respectively [Gan *et al.*, 2017; Gao *et al.*, 2018; Lu *et al.*, 2017; Walia *et al.*, 2013]. In the observation of MoS_2, the vibrational modes E_{2g}^1 and A_{1g} signify in-plane vibration and out-of-plane vibration of Mo and S atoms [Gan *et al.*, 2017; Kumar *et al.*, 2018; Wang *et al.*, 2018a]. It can be observed from Figure 7.4 that A_{1g} vibration mode has a higher intensity than E_{2g}^1 mode, which demonstrates that the nature of as-deposited MoS_2 layers is vertically standing [Kong *et al.*, 2013; Wang *et al.*, 2013a; Wang *et al.*, 2013b].

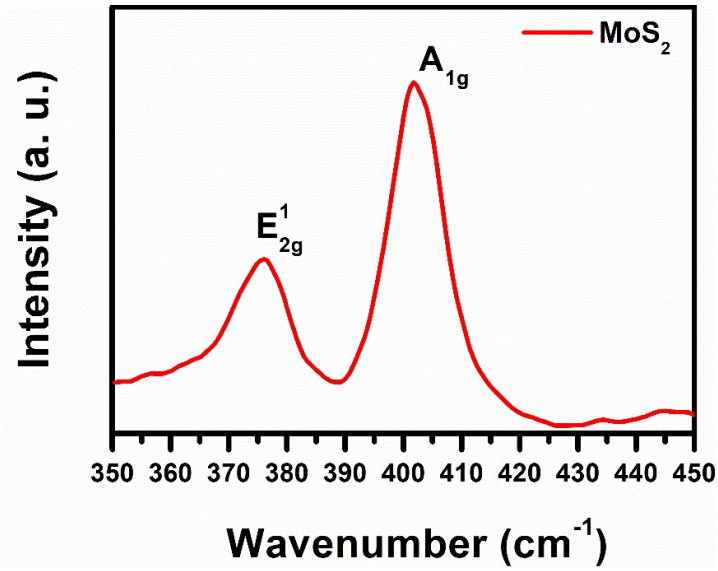

Figure 7.4: Raman Spectrum of as-deposited MoS_2

7.8 STRUCTURAL CHARACTERIZATION OF MoS_2 FUNCTIONALIZED LAYER ON AlGaN/GaN HEMT

The structural characterizations such as FESEM, AFM, and Raman spectroscopy were performed to observe the evidence of the MoS_2 on the gate region of AlGaN/GaN HEMT. These characterizations were executed after drop-casting the MoS_2 on the gate region of AlGaN/GaN HEMT and has shown in Figures 7.5 and 7.6. The FESEM was performed to analyze the morphology of MoS_2 in the gate region. Figure 7.5 (a) and Figure 7.5 (b) shows the lateral and cross-sectional view of MoS_2 functionalized AlGaN/GaN HEMT. Figure 7.5 (a) demonstrates the flower-like structure on the gate terminal of AlGaN/GaN HEMT, where the petals of the flower-like structures are looking vertically standing. The cross-sectional view is shown in Figure 7.5 (b) also confirms the vertical alignment of the petals of the flower-like structure of MoS_2 [Nigam *et al.*, 2020].

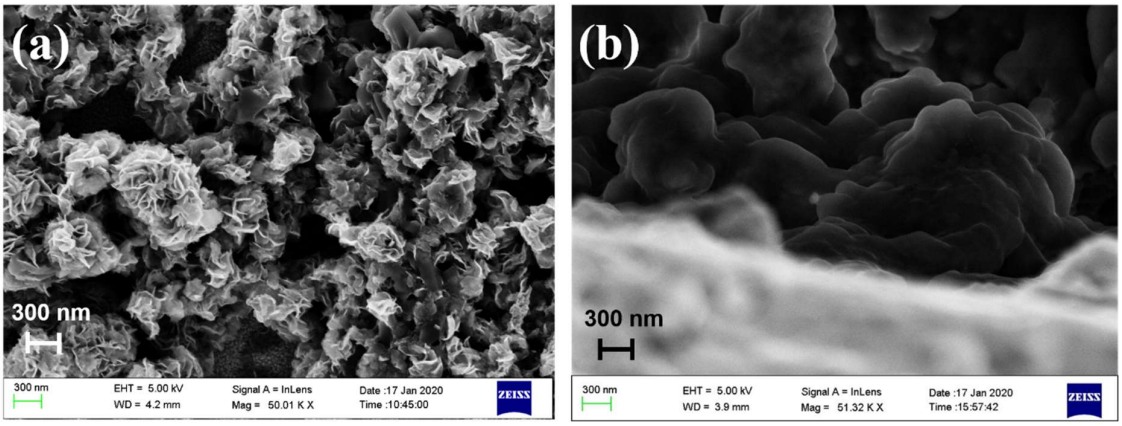

Figure 7.5: (a) FESEM (b) cross-sectional FESEM of the MoS_2 functionalized Au-gated AlGaN/GaN HEMT.

Moreover, AFM analysis was further performed on the device, and the topographical AFM image has been shown in Figure 7.6 (a). The AFM image also reveals the quantitative height

and flower-like morphology on the surface of the Au-gated AlGaN/GaN HEMT. The presence of MoS_2 on the AlGaN/GaN HEMT was further confirmed by utilizing Raman spectroscopy analysis, as shown in Figure 7.6 (b). In this observation, the presence of E_{2g}^1 and A_{1g} vibrational modes was similarly observed as Figure 7.4, which confirms the presence of MoS_2 on Au-gated AlGaN/GaN HEMT. Based on the Raman spectra and the FESEM images, it can be said that the flower-like MoS_2 structures possess rich few-layers structures in the form of petals, which provides a large number of active edge sites [Nigam *et al.*, 2020].

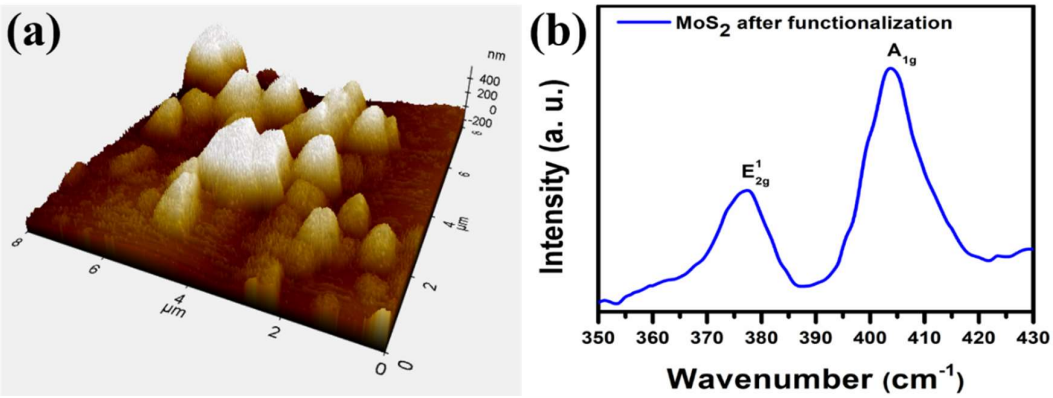

Figure 7.6: (a) AFM images and (b) Raman spectra of MoS_2 functionalized surface of AlGaN/GaN HEMT

7.9 ELECTRICAL CHARACTERIZATION OF MoS_2 FUNCTIONALIZED AlGaN/GaN HEMT FOR Hg^{2+} ION SENSING

The electrical behavior of the fabricated HEMT was examined by measuring drain to source current (I_{DS}) with respect to applied drain to source voltage (V_{DS}), as shown in Figure 7.7. Here V_{DS} was changed from 0 V to 3 V. The I-V characteristics were observed before functionalization (as-fabricated HEMT) after MoS_2 functionalization on the gate terminal, and after applying 10 ppm concentration of Hg^{2+} ions. A distinct variation in I_{DS} can be seen in Figure 7.7 after each step. The I_{DS} was decreased by employing MoS_2 on the gate terminal. It was due to the fact that, when MoS_2 was self-assembled on Au gated region, the metal-semiconductor interface was formed. Since the work function of Au is 5.1 eV, and MoS_2 has ~ 4.7 eV [Goel *et al.*, 2018; Kumar *et al.*, 2018], therefore when the contact is made between MoS_2 and Au, the electrons transferred from MoS_2 to Au due to difference in Fermi levels, which would increase the electrons density in Au.

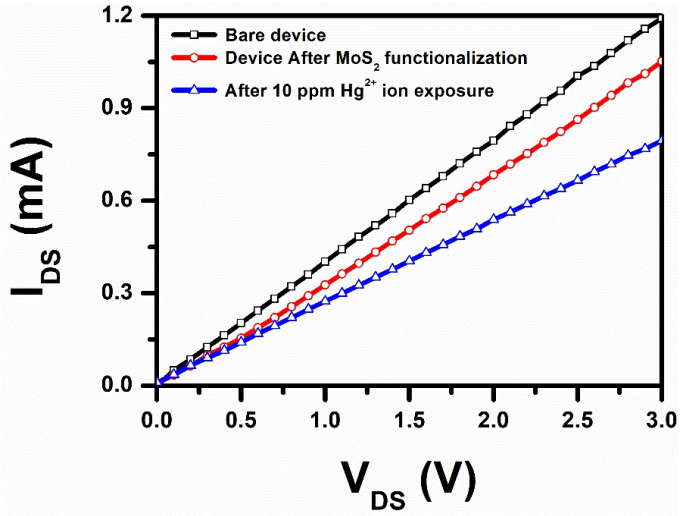

Figure 7.7: I_{DS}-V_{DS} characteristics of the device after different steps of functionalization and sensing.

This excess of electrons increases the negative charge on the Au gated region and make the gate more negative, which ultimately reduce the drain current as follows [Nigam *et al.*, 2020]:

$$I_{DS} = \frac{\varepsilon_n \mu W}{2dL} [2((V_G - V_T)V_{DS} - V_{DS}^2)] \quad (7.2)$$

where ε_n is the total permittivity of GaN cap layer, $Al_{0.23}Ga_{0.77}N$ barrier layer, and AlN spacer layer, V_G is gate potential, W is the width and L is the length of the gate, μ is the electron mobility in 2DEG, V_T is the threshold voltage of the device, and d is the 2DEG and surface distance. The device parameters ε_n, d, L, W, and V_T would be constant.

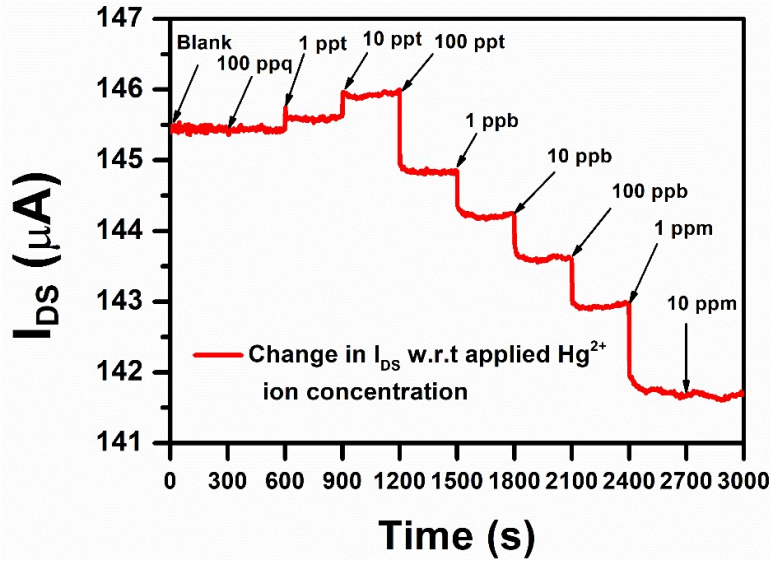

Figure 7.8: Real-time Hg^{2+} ion sensing on MoS_2 functionalized AlGaN/GaN HEMT.

Figure 7.8 showed real-time sensing response of Hg^{2+} ions on MoS_2 functionalized AlGaN/GaN HEMT. In the sensing process, the analysis was carried out by introducing the Hg^{2+} ion solution on the MoS_2 functionalized surface of the gate. Here the concentration of the ionic solution of Hg^{2+} was varied from 0.1 ppt (parts per trillion) to 10 ppm. The sensing response was observed for 300 seconds for each Hg^{2+} ion concentration. After applying different concentrations of Hg^{2+} ions, the apparent variation in the I_{DS} was observed. This alteration in I_{DS} reflects the detection of Hg^{2+} ions [Nigam *et al.*, 2020]. Interestingly, it was found that initially, the I_{DS} was increased by applied Hg^{2+} ion concentration from blank to 10 ppt, and it starts decreasing by applying a higher concentration of Hg^{2+} ions from 100 ppt to 1 ppm.

The reason behind the increment in the drain current could be the electron transfer from MoS_2 to Hg^{2+} due to the chemical adsorption phenomenon. In general, Hg^{2+} ions possess a high binding affinity toward sulfur. When Hg^{2+} ions interact with the sulfur group on the MoS_2 surface, the S^{2-} group may donate electrons to the adsorbed Hg^{2+} ions and make the Hg-S complex with MoS_2 [Jia *et al.*, 2017a; Jia *et al.*, 2017b]. In this process, the negative surface charges decrease, which in turn increases the VG; hence the I_{DS} increases initially by Eq. (7.2). By further increment in Hg^{2+} ion concentration, the drain current starts decreasing. The decrement in the drain current may be observed due to electrostatic interaction at the gate terminal, which induces negative charges towards the MoS_2 functionalized gate region, which can make the gate potential more and more negative, and hence drain current starts decreasing. It can also be seen from Figure 7.8 that after applying a higher concentration of Hg^{2+} ions of 10 ppm, no change was observed in the I_{DS}, which implies that the saturation of MoS_2 functionalized surface due to the higher concentration of Hg^{2+} ions [Nigam *et al.*, 2020].

7.10 CALCULATION OF LIMIT OF DETECTION, SENSITIVITY, AND RESPONSE TIME

The sensing parameters like the limit of detection (LoD) and sensitivity were calculated by observing the I_{DS} vs. Hg^{2+} ion concertation plot, as depicted in Figure 7.9. Here, the limit of detection was calculated by the standard 3-sigma approach, which was described in chapter 1. The limit of detection was calculated by the following expression [Nigam *et al.*, 2020]:

$$\mathrm{LoD} = 3\sigma/\mathrm{m} \tag{7.3}$$

Here σ, and m are the standard deviation (SD) of the least concentration of the Hg^{2+} ions and the sensitivity of the sensor, respectively. The sensitivity (m) of the sensor was calculated as the slope of the fitting curve, and it was observed as 0.64 μA/ppb. The values of parameters such as σ and linear regression coefficient were derived from Figure 7.9 as 0.00246 and 0.9997 respectively, and hence the limit of detection was determined from Eq. (7.3) as 0.01152 ppb or 11.52 ppt. This limit of detection of the Hg^{2+} ions on MoS_2 functionalized AlGaN/GaN is well below the standard limit set by WHO for drinking water standards for Hg^{2+} ions (1 ppb). Thus, it can be said that the sensor is capable of detecting the ultra-low-level concentration of Hg^{2+} ions in the aqueous medium. The linear detection range of the sensor was observed from 0.1 ppb to 100 ppb.

The response time of the sensor was also derived by employing a similar process used in chapter 5. By this process, the sensor demonstrated an ultra-fast response of 1.8 s at 1 ppt[Nigam *et al.*, 2020]. It is the fastest response time observed by MoS_2 functionalized AlGaN/GaN HEMT at a low concentration of Hg^{2+} ions. Thus, the ultra-low-level detection of Hg^{2+} ions with rapid response can be realized using MoS_2 functionalized AlGaN/GaN HEMTs.

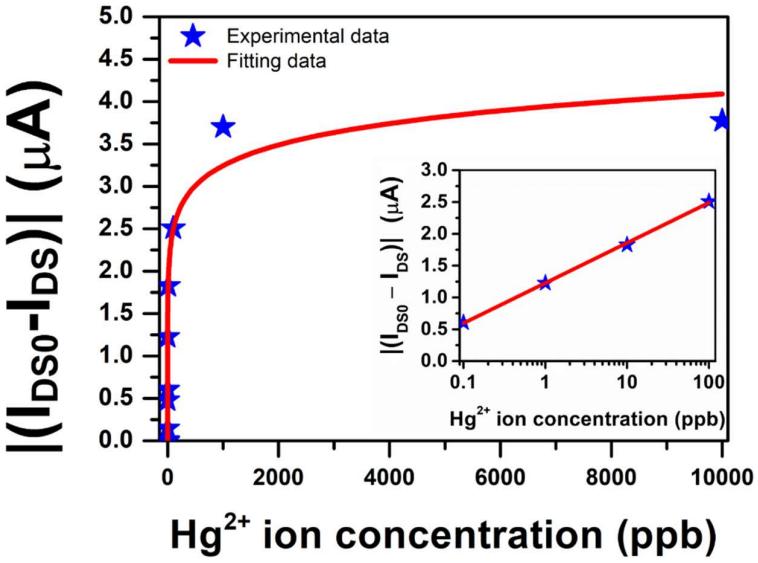

Figure 7.9: Sensor response and calibration curve for Hg^{2+} ion detection using MoS_2 functionalized AlGaN/ GaN HEMT (inset: sensor response at lower concentration)

7.11 SELECTIVITY ANALYSIS OF THE DEVELOPED SENSOR

The selectivity of MoS_2 functionalized AlGaN/ GaN HEMT towards Hg^{2+} ions, and other heavy metal ions were further examined by separate solution method [Maccà and Wang, 1995], and the results are shown in Figure 7.10 (a), (b). In this method, the response of the sensor for Hg^{2+} and other heavy metal ions like Cd^{2+}, Ni^{2+}, Cu^{2+}, Pb^{2+}, Zn^{2+}, and Cr^{3+} was observed at the concentration range from 1 ppt to 10 ppm. For efficient selectivity study, the observed current

response for Hg^{2+} ions and other interfering metal ions were subtracted from the base current, i.e., the I_{DS} observed in deionized water termed as I_{DS0}. Thus, the selectivity coefficient for separate solution approach (also termed as response ratio) $R_{Hg^{2+},j}$ can be given as [Maccà and Wang, 1995]:

$$R_{Hg^{2+},j} = \frac{(|I_{DS0} - I_{DSj}|)C_{Hg^{2+}}}{(|I_{DS0} - I_{DSHg^{2+}}|)C_j} \tag{7.4}$$

where I_{DSj} is the drain to source current of interfering metal ion at concentration C_j, and $I_{DSHg^{2+}}$ is the drain to source current at concentration $C_{Hg^{2+}}$. Here, the sensing response of interfering heavy metal ions and Hg^{2+} ions was measured at an identical concentration of 1 ppm. Hence, the response ratio from Eq. (7.4) can be rewritten as:

$$R_{Hg^{2+},j} = \frac{|I_{DS0} - I_{DSj}|}{|I_{DS0} - I_{Hg^{2+}}|} \tag{7.5}$$

The calculated response ratio from Eq. (7.4) at 1 ppm concentration is shown in Figure 7.10 (b), reveals that the lower the value of $R_{Hg^{2+},j}$, the higher the selectivity. It can be seen from Figure 7.10 (a) that MoS_2 functionalized AlGaN/GaN HEMT sensor showed the measurable response for Hg^{2+} ions, whereas no other meal ions gave any significant response. Further, Figure 7.10 (b) also confirms that the selectivity of the sensor is very high towards Hg^{2+} ions. The high selectivity towards Hg^{2+} ions is observed mainly because of the strong soft–soft interactions between Hg^{2+} ions and S as the metal ions with higher softness have a stronger affinity to sulfur [Ai *et al.*, 2016; Tian *et al.*, 2019]. There was slight interference of Pb^{2+} ions and Cu^{2+} ions, indicates that they are softer than other cations such as Cd^{2+}, Ni^{2+}, and Zn^{2+} ions [Xu *et al.*, 2017]. However, Hg^{2+} ions possess significantly higher softness than $Pb^{2+}$and Cu^{2+} ions [Tian *et al.*, 2019; Xu *et al.*, 2017], which preferably adsorb on the S binding sites and makes the sensor highly selective towards Hg^{2+} ions [Nigam *et al.*, 2020].

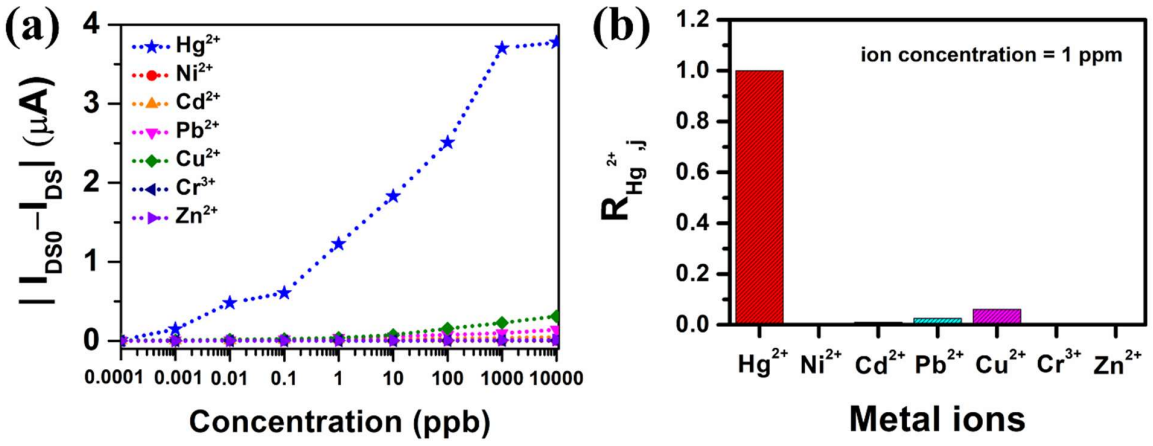

Figure 7.10: (a) Relative sensing response of the sensor for various heavy metal and Hg^{2+} ions from 0.01 ppt to 10 ppm concentration (b) Response ratio of the sensor for Hg^{2+} ions and other interfering heavy metal ions for selectivity analysis.

7.12 ANALYSIS OF RECOVERY, REPEATABILITY, AND REPRODUCIBILITY OF THE SENSOR

The recovery, repeatability, and reproducibility of the AlGaN/GaN HEMT sensor are also important parameters of the sensor and explored here. Figure 7.11 shows the response and recovery of the sensor. In the sensing process, the Hg^{2+} ions were chemically adsorbed on the MoS_2 surface by strong Hg-S bonding. Thus, in order to remove adsorbed Hg^{2+} ions from the surface of MoS_2, more activation energy is required [Sarbu and Sebarchievici, 2017]. Hence, the

PBS buffer was heated at 150°C and applied to the sensor for rinsing [Nigam *et al.*, 2020]. The developed sensor was rinsed in a hot PBS buffer for 100 seconds to recover from the bounded Hg^{2+} ions. During this process, the recovery was achieved by 99.15%. The optimization of the recovery process was performed similarly to our previous report and as explained in chapter 5 [Nigam *et al.*, 2019b]. Thus, it can be said that the utilization of hot PBS buffer provides sufficient activation energy to remove Hg^{2+} ions from the MoS_2 surface, and hence excellent recovery of the sensor was observed.

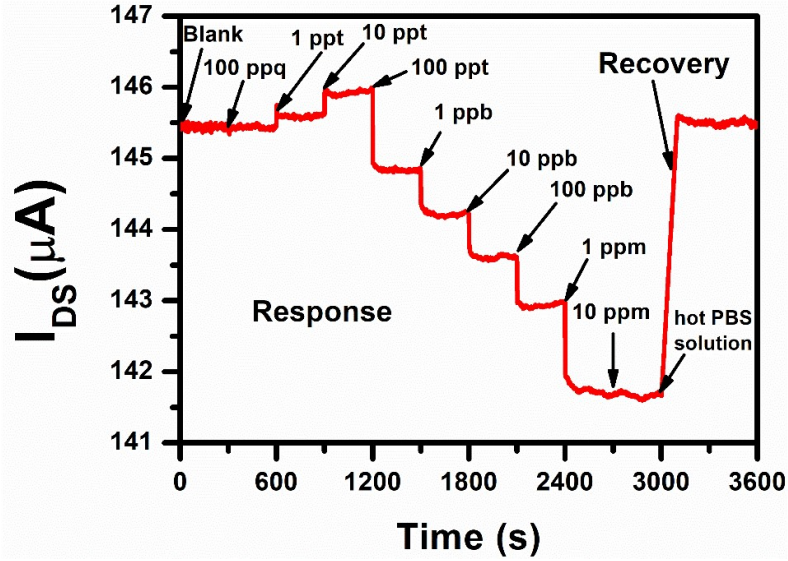

Figure 7.11: Response and recovery of the developed sensor

Furthermore, the repeatability of the sensing response was also observed by keeping all the operating conditions as same as the first sensing response [Nigam *et al.*, 2020]. It has been seen from Figure 7.12 that the sensor showed excellent repeatability of the sensing response under the same operating conditions.

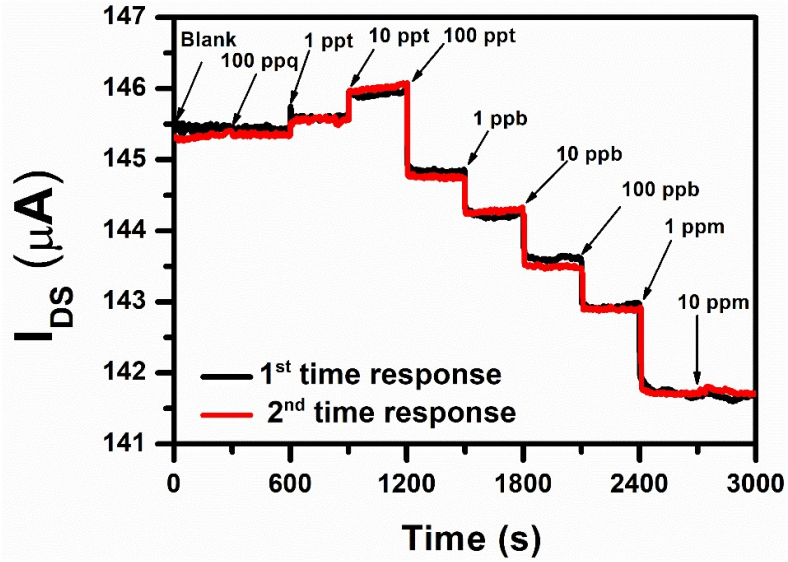

Figure 7.12: Repeatability of the developed Sensor

Moreover, the reproducibility of the sensor was realized by the fabrication of another AlGaN/GaN HEMT device with the same device dimension as a proposed device and keeping the same MoS_2 functionalization process. The sensing analysis was also performed under the same operating conditions as the proposed sensor [Nigam *et al.*, 2020]. The response of the new

device has been shown along with the response of the proposed sensor in Figure 7.13. The slight change in the drain to source current in the new device can be due to the internal resistance of the device. The analysis of the reproducibility of the sensor was conducted by the coefficient of variation (CV) method. The coefficient of variation for both the senor was calculated as [Wang, 2011]:

$$CV = \frac{\text{Standard Deviation of the values of } I_{DS}}{\text{Average of the values of } I_{DS}} \tag{7.6}$$

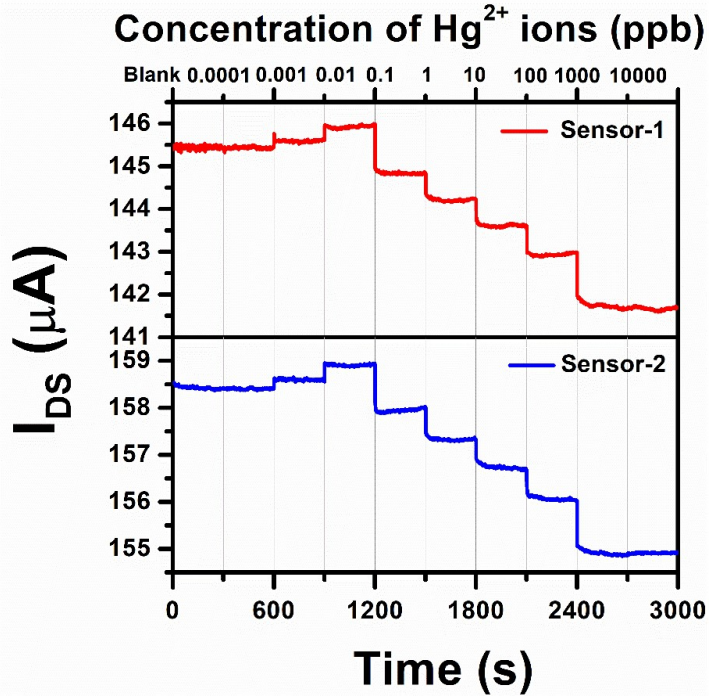

Figure 7.13: Reproducibility of the MoS_2 functionalized AlGaN/GaN HEMT sensor.

Table 7.2 shows the average and standard deviation (SD) of the values of I_{DS} for both the sensors. Here the sensor-1 and sensor-2 are termed as the proposed device and the newly fabricated device, respectively. The calculated values of CV for both the sensor are very close to each other, which indicates the excellent reproducibility of MoS_2 functionalized AlGaN/GaN HEMT sensor for Hg^{2+} ion detection.

Table 7.2: Reproducibility of the MoS_2 functionalized AlGaN/GaN HEMT

Device	*Average I_{DS} (μA)*	*SD of I_{DS} (μA)*	*CV*	*CV (%)*
Sensor-1	144.1428	1.50863	1.05×10^{-02}	1.05
Sensor-2	157.2251	1.42724	9.08×10^{-03}	0.91

7.13 SENSING MECHANISM OF DETECTION OF Hg^{2+} IONS BY MoS_2 FUNCTIONALIZED AlGaN/GaN HEMT

The sensing mechanism of MoS_2 functionalized AlGaN/GaN HEMT for Hg^{2+} ions is shown in Figure 7.14. The functionalized MoS_2 on the Au gated AlGaN/GaN HEMT has exposed Sulfur atoms to attract the Hg^{2+} ions, as shown in Figure 7.14 (a). When the device was exposed to the Hg^{2+} ion solution, Hg^{2+} ions were strongly adsorbed on the surface of MoS_2. Initially, Hg^{2+} ions adsorb on the most sites on the MoS_2 surface and form Hg–S complexation, as shown in Figure 7.14 (b). This formation of chemical complexion is kept going on until Hg^{2+} ions fully

occupy the binding sites of the MoS_2 functionalized surface. In this process, the reduction of Hg^{2+} ions may occur on the surface of MoS_2 by Sulfur (S) as Hg^{2+} ions are the strong oxidizing agent while S is a natural reducer. Thus, the S^{2-} in MoS_2 can donate its electrons to interact with Hg^{2+} ions to form Hg-S complex [Aswathi and Sandhya, 2018; Jia *et al*., 2017b]. Hence, the formation of the Hg-S complex ultimately reduces the electrons from the MoS_2 surface, which in turn increases the gate potential of the device, and hence the I_{DS} rises.

By further increment in Hg^{2+} ions concentration, the binding sites on the top of the first Hg^{2+} ion layer can be further engaged by Hg^{2+} ions, which can also form the second Hg^{2+} ions layer. It is because the MoS_2 may still have negative charges due to higher S atoms and n-type behavior, and the physical electrostatic interaction phenomenon causes further Hg^{2+} ions adsorption, as depicted in Figure 7.14 (c). The electrostatic interaction further induces negative charges towards the MoS_2 surface. Thus, while increasing more Hg^{2+} ion concentration, more negative charges induce towards MoS_2 surface. This process decreases the gate potential simultaneously, and hence, I_{DS} starts reducing by a further increase in Hg^{2+} ion concentration. Some reports have reported that the MoS_2 layer was negatively charged in the complete sensing process; only the potential associated with MoS_2 would be less or more negative [Jia *et al*., 2017a; Jia *et al*., 2017b]. Thus, these two-adsorption mechanisms can happen one after another to unwrap the role of MoS_2 for ultra-low-level determination of the Hg^{2+} ions. In addition to the affinity of Hg^{2+} ions to the MoS_2 surface, the ultrahigh surface to volume ratio and the electronic transport properties of MoS_2 may also fasten the Hg-S complex formation and electrostatic interaction appearing over the gate terminal [Nigam *et al*., 2020]. Hence the AlGaN/GaN HEMT with MoS_2 functionalization provides an ultra-fast response for the detection of Hg^{2+} ions.

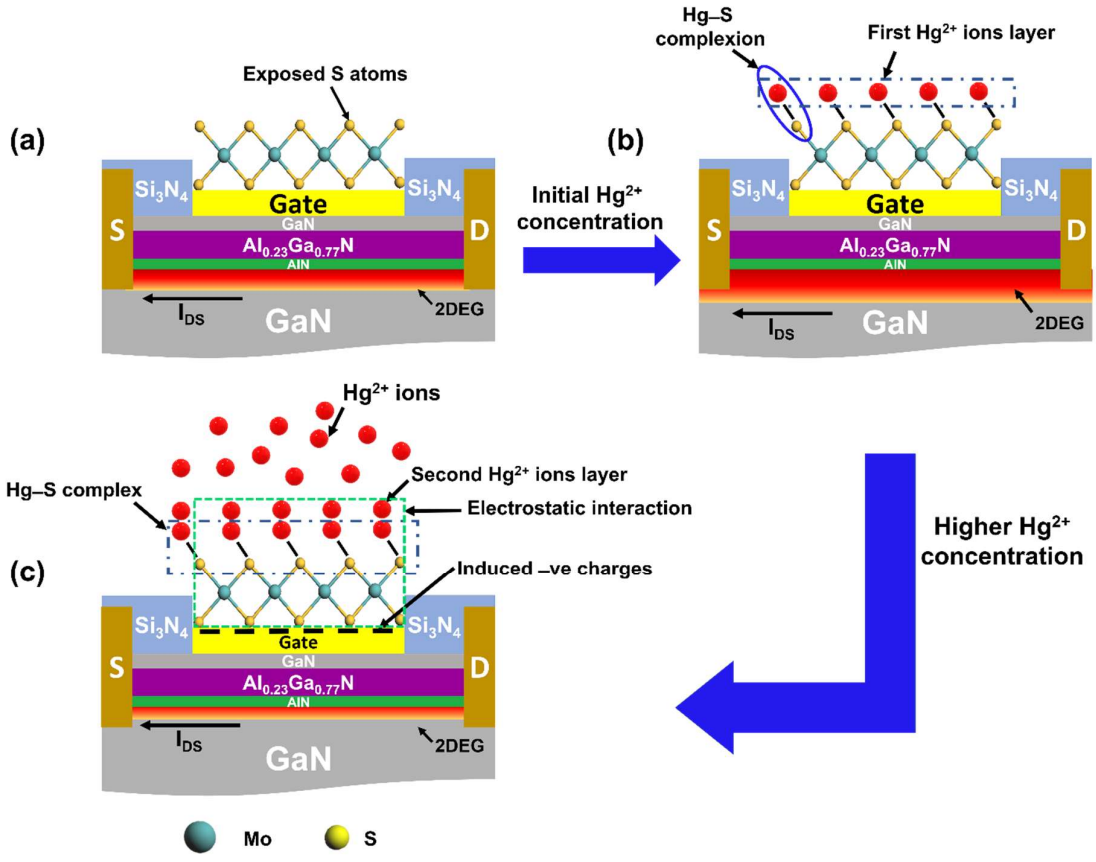

Figure 7.14: Sensing mechanism of MoS_2 functionalized AlGaN/GaN HEMT for Hg^{2+} ion detection (a) HEMT with MoS_2 functionalization (b) Hg-S complex formation on the gate region of HEMT at low concentration of Hg^{2+} ions (c) electrostatic interaction between Hg^{2+} ions and MoS_2 layer at high concentration of Hg^{2+} ions.

7.14 COMPARISON OF DEVELOPED Hg^{2+} ION SENSOR WITH OTHER METHODOLOGIES

The performance of the proposed MoS_2 functionalized AlGaN/GaN HEMT sensor was compared with previously reported Hg^{2+} ion sensors and showed in Table 7.3. The comparative analysis was made in terms of limit of detection of the sensors and their response time for Hg^{2+} ion detection, observed that the MoS_2 functionalized AlGaN/GaN HEMT showed excellent detection limit with rapid response time as compared to previously reported Hg^{2+} ion sensors.

Table 7.3: Comparison of different sensing techniques for Hg^{2+} ion detection

Methods	Functionalization	LoD (ppb)	Response time	References
ISFET	rGO/TGA-AuNP	5	< 10 s	[Chen *et al.*, 2012a]
SERS	Mesna/ AgNP	0.0024	9 min.	[Chen *et al.*, 2012b]
Colorimetry	DMSO: water	1	–	[Udhayakumari and Velmathi, 2013]
Electrochemical	L-cysteine	0.995	–	[Muralikrishna *et al.*, 2014]
Electrochemical	CB/SPE	1	< 3 min	[Arduini *et al.*, 2011]
AlGaN/GaN HEMT	TGA/Au	27; 3	5 s; 15-20 s	[Chen *et al.*, 2008; Wang *et al.*, 2007]
AlGaN/GaN HEMT	PVC	2	–	[Asadnia *et al.*, 2016]
AlGaN/GaN HEMT	MoS_2/Au	0.01152	1.8	This work

rGO: reduced graphene oxide; TGA: thioglycolic acid; AuNP: gold Nanoparticle; AgNP: Silver Nanoparticle; Mesna: sodium 2-mercaptoethanesulfonate; SERS: Surface Enhanced Raman Spectroscopy; DMSO: dimethyl sulfoxide; CB/SPE: carbon black/ screen-printed electrode; Polyvinyl chloride.

7.15 CONCLUSION

In summary, the flower-like structures of MoS_2 have been successfully synthesized using the hydrothermal process. The morphology, structural properties, and quality of synthesized MoS_2 were characterized through microscopic and spectroscopic measurements. Moreover, we have proposed, for the first time, the hydrothermally prepared MoS_2 flower-like structure functionalized AlGaN/GaN HEMT for toxic Hg^{2+} ion detection. Interestingly, the device shows a rapid response time of 1.8 s and an excellent detection limit of 11.52 ppt. The proposed sensor demonstrates excellent selectivity towards Hg^{2+} ions. The possible reasons for the outstanding sensitivity were Hg-S complex formation due to interactions between the S of MoS_2 at low concentration of Hg^{2+} ions and the electrostatic iteration between MoS_2 and Hg^{2+} ions at high concentration of Hg^{2+} ions. Thus, the superior binding properties of MoS_2 for Hg^{2+} ions with an ultra-high surface to volume ratio in conjunction with AlGaN/GaN HEMTs makes the feasibility of highly selective and sensitive Hg^{2+} ion sensor with ultra-low-level detection and rapid response time.

…